

Turbulent layering beneath the pycnocline in a strongly stratified pit lake

Craig L. Stevens¹

National Institute for Water and Atmospheric Research, Greta Point, P.O. Box 14-901, Kilbirnie, New Zealand

Timothy S. R. Fisher² and Gregory A. Lawrence

Department of Civil Engineering, University of British Columbia, Vancouver, BC V6T 1Z4, Canada

Abstract

Temperature microstructure observations from a pit lake show alternate layers of high and low turbulence beneath a very strong pycnocline. The layers were clearly defined, around 0.3–0.5 m thick, and were found both at the edge and in the center of the pit lake. In the most energetic regions, the turbulent energy dissipation rate reached $\varepsilon = 10^{-6} \text{ m}^2\text{s}^{-3}$ and the dissipation rate of thermal variance almost reached $\chi_\theta = 10^{-4} \text{ }^\circ\text{C}^2\text{s}^{-1}$. The turbulent fluid in the middle of the lake had a higher dissipation ratio, the thermal component of potential energy gain vs. kinetic energy loss, when compared with the sidewalls. This is attributed to different forcing mechanisms for the turbulence. We hypothesize that basin-scale internal waves, in conjunction with the topography, create sidewall boundary layers. In the interior regions of the pit lake, the turbulent layers are probably generated by instability due to focusing of short-wavelength internal waves.

A pit lake is a water body that forms in a mining void on the cessation of mining activity. Usually a lake only forms in regions where the accumulation of groundwater inflow and rainfall exceed evaporation. Alternately, the pit lake can be actively filled as an aid to remediation or for storage. Some of the dissolved material that finds its way into a pit lake is environmentally undesirable (Klapper and Schultze 1995). The potential for a wide range of physical transport rates means there is a growing awareness of the importance of understanding the hydrodynamics of such environments. Most pit-lake observational studies to date severely test the notion of simply treating a pit lake as a natural lake. Facets like site-specific equations of state (Karakas et al. 2003; Fisher and Lawrence in press), ground water fluxes (Boehrer et al. 1998), wall subsidence (Stevens and Lawrence 1998), highly variable inflows (Stevens and Lawrence 1997a), and sun and wind wall-sheltering (Hamblin et al. 1999) drive significant departures from lake-like behavior.

Because of the elevated levels of dissolved material many pit lakes are meromictic—they do not completely mix vertically at anytime throughout the seasonal cycle. Meromixis in natural freshwater lakes usually requires some significant event to provide dissolved material to resist thermal turnover (e.g., remnant seawater; Sanderson et al. 1986). Saline lakes readily become meromictic with the addition of freshwater (e.g., MacIntyre et al. 1999). Strong, persistent density in-

terfaces associated with meromixis are regarded as essentially capping the deeper fluid and so isolating the fluid beneath from the energy fluxes at the water surface and thus minimizing diffusive transport rates. Here we describe data that suggest care needs to be taken in assuming this is always the case.

From the perspective of long-term modeling of vertical transport of contaminants (Hamblin et al. 1999), one focuses on the vertical turbulent diffusivity coefficient of some given material K_z . Although broad empirical estimates of K_z exist, it is important to be mindful that we are considering long timescales of perhaps 50 yr or more (Stevens and Lawrence 1997a) in relatively undersampled and unique systems. Consequently, it is important to develop some mechanistic basis for our understanding before developing an averaged empirical picture (see also Ruddick et al. 1997).

A direct estimate of vertical diffusion of temperature K_θ can be derived from the dissipation of thermal variance, $\chi_\theta = 6D_\theta \langle \partial\theta'/\partial a \rangle^2$ (where D_θ is the coefficient of molecular diffusion of heat, $\langle \rangle$ denotes a bin average and $\partial\theta'/\partial z$ is the perturbation in vertical gradient of temperature) so that

$$K_\theta = \frac{\chi_\theta}{2\langle \theta_z \rangle^2} \quad (1)$$

where θ_z is the vertical temperature gradient. However, K_θ is often difficult to determine in field situations because vertical temperature gradients in surface layers and hypolimnia are so weak (see Sherman and Davis [1995] for discussion in an oceanic context) and many profiles are required to resolve K_θ .

Alternately the vertical eddy diffusion of buoyancy may be cast in terms of the strength of the stratification and the turbulent kinetic energy (TKE) of the flow as quantified by the dissipation rate of TKE (ε) so that (Osborn 1980)

$$K_\rho = \Gamma \frac{\varepsilon}{N^2} \quad (2)$$

where Γ is a coefficient and the buoyancy frequency N is

¹ Corresponding author (c.stevens@niwa.cri.nz).

² Present address: Tonkin and Taylor Ltd., Auckland, New Zealand.

Acknowledgments

This work was supported by the New Zealand Royal Society administered Marsden Fund, the New Zealand Foundation for Research Science and Technology and the Canadian Natural Sciences and Engineering Research Council. Bertram Boehrer and BHP-Billiton provided assistance with the data collection and Michael Head provided support for the PME SCAMP microprofiler. We also wish to acknowledge the useful comments made by two anonymous referees.

given by $N^2 = (g/\rho_0)d\rho/dz$ (g is gravitational acceleration, ρ_0 is an average density, and $d\rho/dz$ is the local density gradient). Osborne (1980) determined that $\Gamma \leq 0.2$, but it is often set as a constant $\Gamma = 0.2$ (Sharples et al. 2003). Setting $K_\theta = K_\rho$ results in

$$\Gamma = \frac{\chi_\theta N^2}{2\theta_z^2 \varepsilon} \quad (3)$$

Thus, Γ is a dissipation ratio (St. Laurent and Schmitt 1999) or dissipation flux coefficient (Moum 1996) and can be viewed as a parameter gauging the gain of potential energy relative to loss of kinetic energy (Ivey and Imberger 1991). The observed value of Γ , denoted Γ_d , is seen to vary by orders or magnitude in an instantaneous sense (Gargett and Moum 1995; Moum 1996; Stevens 2003). Furthermore, here we consider only the temperature component of the gain in potential energy associated with temperature alone in a system where stratification is dominated by salinity and so we relabel (2) as Γ_d^θ . Nash and Moum (2002) found the salinity equivalent to Γ_d^θ , measured in an oceanic environment, to be of a similar magnitude. By definition, active microstructure occurs at scales largely unaffected by buoyancy, so that $K_z \sim K_\theta$.

The observations are from the Island Copper pit lake, near Port Hardy, British Columbia, Canada. This pit lake is unusual in that, in 1996, it was initially filled with seawater, which was then covered naturally by a precipitation-induced thin, relatively fresh, surface layer above the seawater. An exceptionally strong pycnocline separated the two layers. Fisher and Lawrence (in press) describe a long-term study examining aspects of the bulk stratification evolution. The present paper describes, as far as the authors are aware, the first temperature microstructure observations in a pit lake. The observations of the mixing activity show unusual features that shed light on the energy regimes beneath strong pycnoclines.

Methods

The Island Copper mine pit lake is located on Rupert Inlet near Port Hardy on Vancouver Island, British Columbia, Canada ($50^\circ 36'01''\text{N}$; $127^\circ 28'26''\text{W}$). The basin is around 1.5 km in diameter at the water surface and almost 400 m deep (Fig. 1). The true bathymetry was more complex than indicated in Fig. 1 because of the pit bench structure. The benches were 12.2 m high and wide, with some double-height benches that were 24.4 m high and 12.2 m wide. The benches were essentially flat when constructed. However, prior to inundation, waste rock was pushed into the pit lake on the south wall and, since inundation, slope failures and weathering have smoothed out the bench structure to the extent that, at the time of the observations, the pit walls deviate from the bench structure for approximately a third of the perimeter. A bench coincided with the pit lake's ultimate water level (UWL, 2.44 m above mean sea level). The present observations were recorded in July 2000, at which time the surface water level was 0.15 m below the UWL. This placed the pycnocline (7.4–8.5 m below UWL during December 1999–November 2000) some 4 m above a

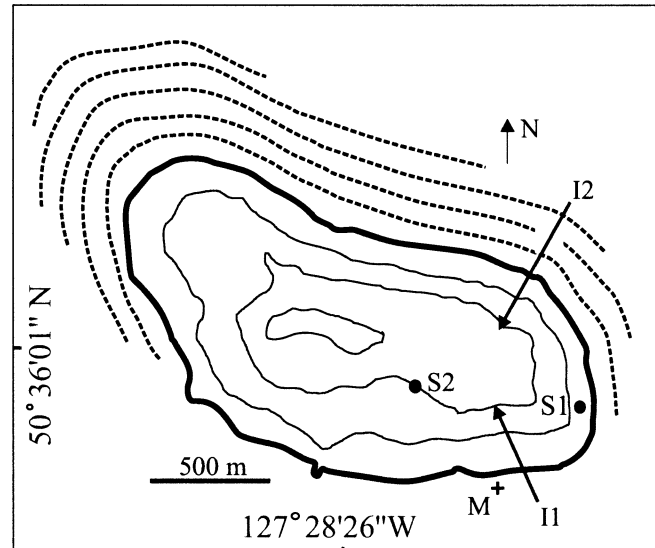


Fig. 1. Island Copper pit lake bathymetry. The bold black line is the water-surface boundary, the thin black lines are bathymetric contours at 100-m intervals. The dotted lines represent bench lines at 12-m intervals above the water surface. The microstructure sampling Stas. were S1 and S2. Runoff from the region during periods of rainfall are collected and injected into the pit lake near the bed at I1 and I2. It did not rain in the period prior to or during our sampling. Meteorological data, including wind speed, wind direction, air temperature, and solar radiation were recorded on shore at location M.

bench, and therefore exposed to essentially a vertical rock wall or steeply sloping rubble surface. However, there was still stratification at the depth of the bench step.

Meteorological data, including wind speed, wind direction, air temperature, and solar radiation were recorded on shore at location M (Fig. 1). Rainfall runoff injection points into the lake were located near the bed at I1 and I2. There was no rainfall immediately prior to or during our sampling, so mixing due to injection is not treated here (instead, see Fisher and Lawrence in press). Temperature time series (30-s sampling interval) were recorded with suspended thermistors near S1 and S2.

Temperature-gradient microstructure data were acquired using SCAMP, a loose-tether instrument (Ruddick et al. 2000) with the primary measured parameter being the analog-derived temporal gradient of temperature, which can be converted into a spatial gradient (θ_z) using the drop-speed and then filtered to give mean and perturbation components. The main microstructure sampling took place on 05 and 06 July 2000, with follow-up winter observations recorded during 21–23 January 2002. The majority of the measurements were recorded at Stas. S1 and S2 (Fig. 1). Profiles were repeated at the same station at around 6-min intervals. The boat was not moored, so the vessel drift in the slight breeze and the occasional repositioning minimized the likelihood of profiling through the wake of previous profiles.

This profiler also measured conductivity at a resolution comparable with the temperature measurements, enabling an estimate of density to be calculated. The equation of state was assumed to be that of seawater, although it is clear that

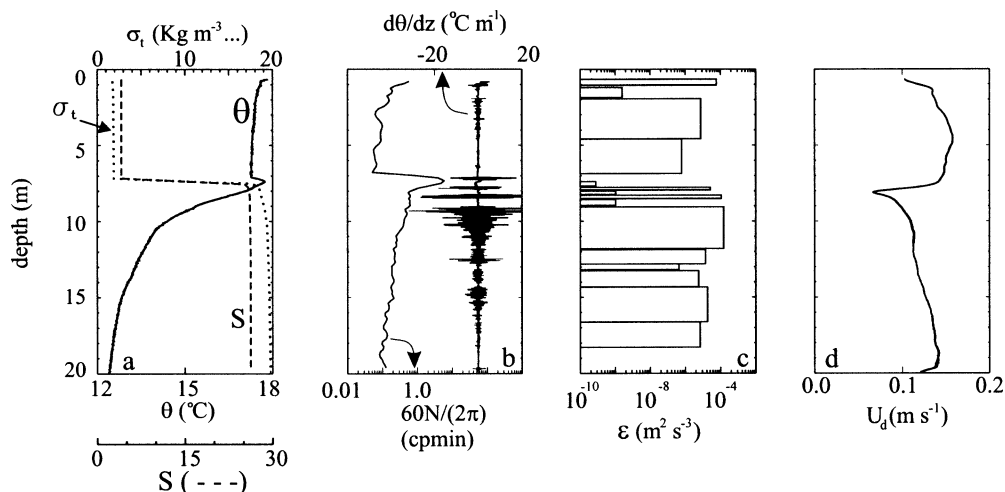


Fig. 2. Typical stratification from a profile recorded at Sta. S1 on 06 July 2000 at 1357 h. Properties from a section of a single profile showing (a) temperature, θ ; salinity, S ; and density ρ_t , 1,000; referenced to air pressure. The corresponding (b) buoyancy frequency N and high-passed (cutoff at the bin scale) vertical gradient of temperature ($d\theta/dz$), (c) segmented energy dissipation rate estimate ε , and (d) profiler fall speed.

this is only indicative in such systems (Gräfe et al. 2002; Karakas et al. 2003; Fisher and Lawrence in press). The buoyancy frequency was derived using the bin-averaged (128 point, equivalent to 0.12 m) density gradient.

The Cox number $C'_z = \langle \theta'_z \rangle^2 / \langle \theta_z \rangle^2$ (where the prime and overbar refer to perturbation and mean values) provides a measure of the strength of turbulence relative to stratification (Dillon and Caldwell 1980). The temperature gradient data enabled estimates of C_x , turbulent energy dissipation rate ε (Oakey 1982; Ruddick et al. 2000), and diffusivity of temperature K_θ with the same bin size as N . Kocsis et al. (1999) have demonstrated that temperature microstructure dissipation estimates are comparable with those resolved using shear microstructure. Furthermore, Etemad-Shahidi and Imberger (2001) have shown this approach to have the lowest noise floor of any dissipation rate estimator. Small bins (128 points) were used to calculate most properties. However, for ε and χ_θ , we used the stationarity-based segmentation method described in Imberger and Ivey (1991), resulting in variable bin size. Use of a small fixed bin size introduces a wave-number limitation that would bias the ε estimates high in the narrow, low-energy bands observed here.

Results

The most striking initial observation was the strength of the stratification at the top of the pycnocline (depth of 7.4 m; Fig. 2a), which was dominated by salinity stratification. In the apparent absence of strong stirring, the buoyancy frequency reached 0.1 Hz (6 cpm; Fig. 2b). While estuarine systems maintain comparable buoyancy frequencies (Sharpley et al. 2003), this is through replacement of water and constant highly energetic benthic stirring. The stratification resulted in a region of low turbulent kinetic energy (7.5 m, Fig. 2c). Furthermore, so great was the stratification in the pit lake that the microprofiler free-fall drop speed (Fig. 2d)

would decrease to as little as half its initial value, prior to a slow recovery to a drop speed of around 75% of the upper-layer drop speed (Srdic-Nitrovic et al. 1999). We attribute this velocity minimum to generation of internal waves by the sharp-edged profiler drag plate rather than a direct buoyancy-modulated sinking effect.

Beneath this very strong stratification was a region of only moderate stratification but which sustained bands of high and low turbulent energy dissipation rate, ε , indicating regions of enhanced mixing relative to that expected beneath such a strong pycnocline. Circumstantial evidence for this enhanced mixing is found in the nature of the temperature profile in this region (>7.4 m; Fig. 2b), which exhibited perturbations from the smooth distribution expected if molecular diffusion were controlling transport (Fig. 2a). Direct evidence for this enhanced mixing was found in the temperature-gradient signal, where the region beneath the pycnocline was characterized by the appearance of layers of energetic turbulence separated by very well-defined regions, around 0.3–0.5 m thick, that were essentially laminar. Beneath a depth of around 9.5 m, the turbulence was weaker but more persistent and continuous with depth. In this region, the double-sided temperature gradient signal decreased with depth, as would be expected for constant TKE in a decreasing background temperature gradient.

Sequences of microstructure profiles at S1 and S2 (S1, Fig. 3; S2, Fig. 4) reveal the consistency of the turbulent and quiescent layers. The quiescent layers centered at 8.0 and 8.8 m were more consistent at S1 than in the center of the lake at S2. The time-averaged temperature profiles at S1 and S2 are similar, which enables Figs. 3b and 4b to be compared directly, assuming the turbulence beneath the pycnocline is not directly forced by the wind (see *Discussion*). As well as S1 sustaining less turbulent gradient signal, it is clear that the quiescent bands were more persistent at this site than at S2, although the turbulent profiles cannot be

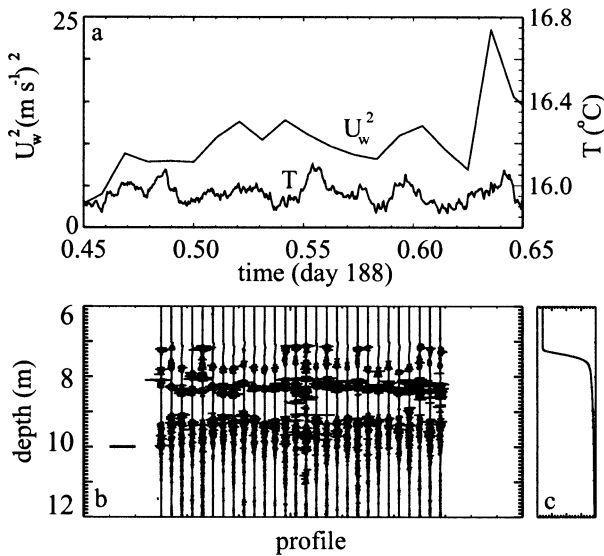


Fig. 3. Sidewall data (Sta. S1) showing (a) temperature time-series (8.55 m depth) and wind speed squared recorded at Sta. M on the pit shoreline. (b) Offset perturbation temperature gradient profiles (the horizontal bar is $100^{\circ}\text{C m}^{-1}$ long), the top of the pycnocline is at around 7.4 m, as shown in the density profile to the right (extending from 0 to 20 kg m^{-3}). The profiles in panel (b) align with times in panel (a).

directly linked with changes in the local moored thermistor trace (Fig. 4a). The displacements inferred from the moored thermistors, using the average temperature profile as a reference, suggest vertical excursions at the sidewall Sta. S1 of around 0.1 m and perhaps half this at S2. As a result, the

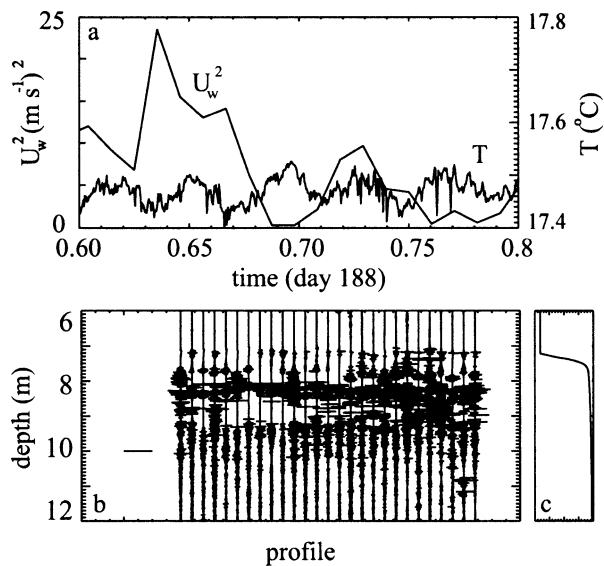


Fig. 4. Lake-central data (Sta. S2) showing (a) temperature time-series (8.0 m depth) and wind speed squared recorded at Sta. M on the pit shoreline. (b) Offset perturbation temperature gradient profiles (the bar is $100^{\circ}\text{C m}^{-1}$ long, the top of the pycnocline is at around 7.4 m, as shown in the density profile to the right (extending from 0 to 20 kg m^{-3}). The profiles in panel (b) align with times in panel (a).

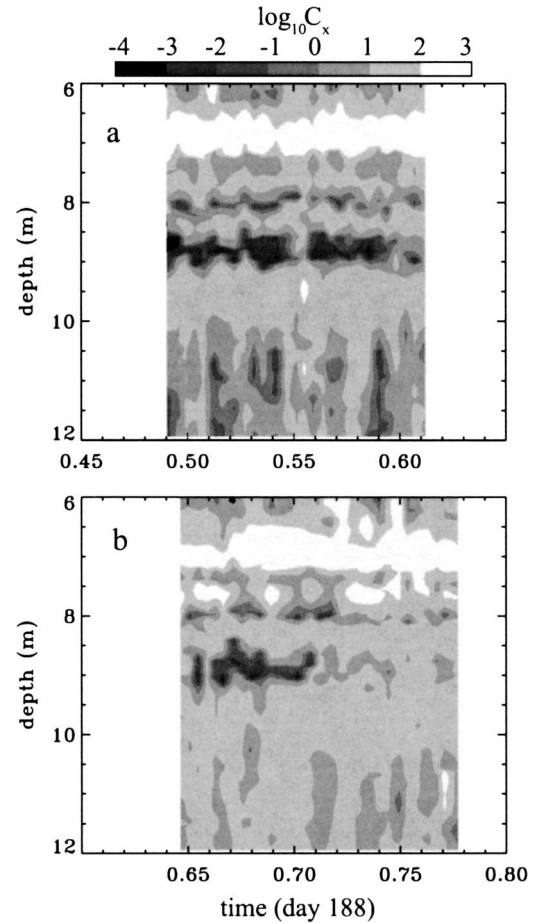


Fig. 5. Contours of the $\log_{10} C_x$ at (a) Sta. S1, the sidewall, and (b) Sta. S2 in the center of the pit lake.

S1 ϵ levels were highly variable when compared with the data from the central Sta. S2.

At S1, the layer at 8.8 m was disturbed for a couple of profiles near the middle of the period (time $t = 0.55$; decimal day 188), which corresponded to a period of change in temperature at the near-by moored thermistor (Fig. 3a). However, similar elevated temperature gradients were not seen at other times of rapid temperature change ($t = 0.49$ and $t = 0.58$). At the sidewall Sta. S1, mixing events at the upper side of the pycnocline were apparent (Fig. 3b, depth = 7.2 m), indicating interfacial instability.

The temperature gradient profiles in the center of the lake sustained larger C_x levels (Fig. 5). Furthermore, at S2, the erosion of the layers can be seen along with the more consistent turbulent kinetic energy below 10 m. The marked differences between Figs. 3 and 4 are deemphasized in the log scaling C_x in Fig. 5. The elevated C_x at the pycnocline for both stations was due to the temperature inversion seen in Fig. 2a. A similar temperature inversion was also seen in Brenda Mines pit lake (Stevens and Lawrence 1998). Beneath this, there was a general elevation in C_x at S2. Dillon and Caldwell (1980) estimated C_x in a wind-driven oceanic surface layer to be in the range 10^0 – 10^5 . The present results are generally smaller than this, with the values in the quiescent layers being as much as three decades smaller.

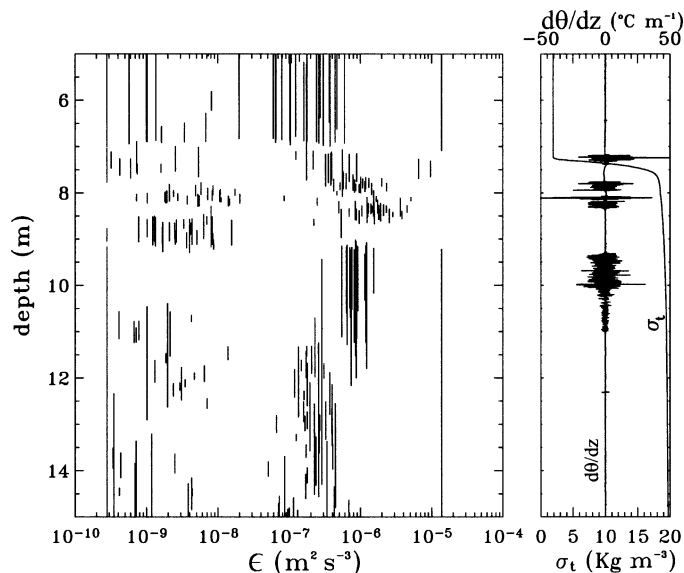


Fig. 6. Dissipation rate segments from the sidewall Sta. S1. The left-hand panel places all segments as bars extending over their profile location. The right-hand panel is a single profile of density and perturbation temperature gradient from the middle of this profile sequence.

The variability of the energy dissipation rate estimates is visualized in Fig. 6. This shows the spatial extent and magnitude of the dissipation rate in the various segments. We propose that this is an important extension in the visualization of such data because it illustrates the variability that is either not captured in single profiles or removed in bin averages that are heavily biased toward the larger events. The base of the surface layer was reasonably consistently between $\epsilon = 0.6\text{--}8 \times 10^{-7} \text{ m}^2 \text{ s}^{-3}$, while the region just below the interface (7.25–7.5 m) sustained slightly greater ϵ . Beneath this were four clear layers of alternating energy levels, with the turbulent layers at around $\epsilon = 10^{-6} \text{ m}^2 \text{ s}^{-3}$ (layer centers at 7.8 and 8.4 m depth) and the quiescent layers

closer to $\epsilon = 5 \times 10^{-9} \text{ m}^2 \text{ s}^{-3}$ (centers at 8.1 and 8.8 m). The dissipation rate in the deeper portion of the water column decreased from $\epsilon = 8 \times 10^{-7} \text{ m}^2 \text{ s}^{-3}$ to $\epsilon = 5 \times 10^{-7} \text{ m}^2 \text{ s}^{-3}$ (beneath 9 m). Note the two large segments at $\epsilon = 1.5 \times 10^{-5} \text{ m}^2 \text{ s}^{-3}$. It appears as if these were saturated results—potentially from profiling through the wake of a previous profile. These totally dominate any arithmetic mean and have been discarded at least for the present consideration.

Having identified the intermittent nature of the flow, now we can turn to the bin averages. Small bins have been used to try and maintain the coherency of the turbulent and quiescent layers. By moving through each profile and adding to the running means of all bins falling within the segment, it is possible to build up a temporal average. In terms of ϵ , there are only moderate differences between stations (Fig. 7), with the sidewall station maintaining slightly lower ϵ in the surface layer and a higher ϵ between 9 and 10 m depth. The clearest difference lies in the χ_θ data at depths greater than around 11 m, with the central data sustaining χ_θ almost three times larger than the sidewall data. Note that a bench step lies at a depth of around 12 m.

Discussion

The energetic mixing beneath the pycnocline, manifest in the turbulent layers, is intriguing and generates a number of questions. First, are they real? If so, are the dissipation rate measurements within them reliable? Second, what causes the layers? Finally, how do these mechanisms relate to what happens in a natural lake?

Measurement reliability—A number of issues point to the veracity of the measurements of the turbulent layering. They were not an effect of previous sampling because they were observed in single casts at locations across the pit lake well away from previous profiles. Also, they were not thought to be a profiler–stratification interaction because of their vari-

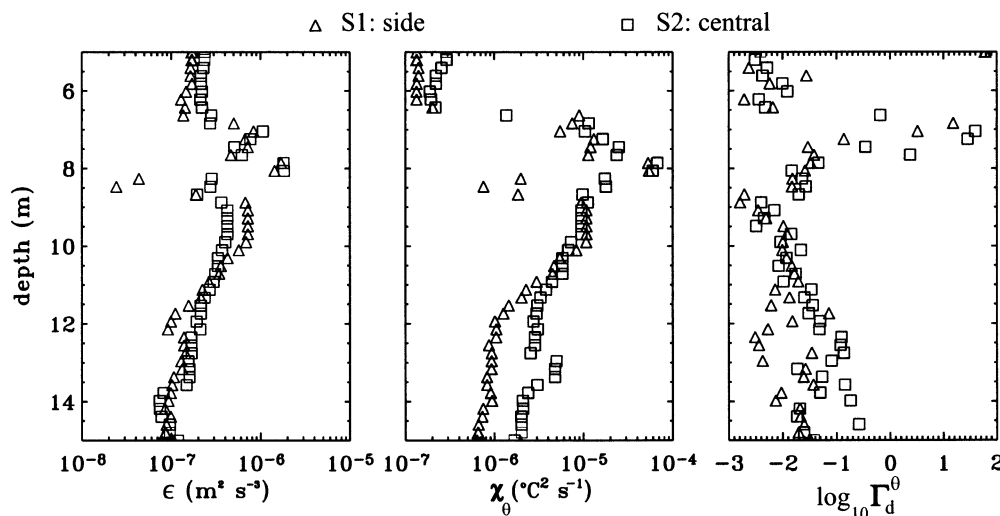


Fig. 7. Profiles of temporally averaged (binned) (a) TKE dissipation rate, ϵ ; (b) dissipation rate of thermal variance, χ_θ ; and (c) \log_{10} of dissipation ratio Γ_d^θ at S1 and S2.

able nature and they were often seen more than two profiler lengths from the pycnocline. Furthermore, they were not seen by Sharples et al. (2003) under reasonably similar stratification, nor were they observed during the Island Copper winter sampling of 2002. If the bands had been caused by some sort of stratification–instrument interaction, they would have been seen at these times.

We can identify a number of possible explanations for the nonappearance of the turbulent layers in the 2002 winter observations. There were differing wind histories for the two experiments. There would have been greater prior injection inflow that might have engulfed the layers, except that the turbulence levels were somewhat lower in the winter sampling. The pycnocline was somewhat closer to the surface in the 2002 observations, which would have moved it even further from the bench step.

With respect to the reliability of the ε estimates, Sharples et al. (2003) attributed a spike in dissipation rate just beneath the pycnocline to sensor rotation as the drag plate passed through the pycnocline. There is some evidence of the spike in dissipation just beneath the pycnocline seen by Sharples et al. (2003). For example, one of the largest dissipation rates estimated in Fig. 2c was indeed just beneath the pycnocline, but this was not always the case. Potentially, the quiescent nature of pit lakes in terms of horizontal currents results in the profiler crossing the interface at a near-normal angle, so reducing any oscillatory response that might lead to artificially increased wave numbers. The bias appears to be at most an order of magnitude in that one sample bin and, when averaged over any significant depth (say 8–20 m), will have minor influence. The drop in profiler speed was presumably due to wave drag as the profiler drag plate moved through the pycnocline. The microstructure sensors are 500 mm in advance of the drag plate, and so these measurements were unaffected except in the changing spatial response. The extent of each individual segment was related to signal stationarity and so did not cross layer boundaries.

While the vertically averaged dissipation rate is relatively constant (even the sidewall average varies by less than a decade), the dissipation profiles that make up these averages often varied by over three decades. The arithmetic vertical average was dominated by perhaps one or two high values. In other words, some profiles sustained, say, $\varepsilon = 5 \times 10^{-7} \text{ m}^2 \text{ s}^{-3}$ for most of the region, whereas in other profiles, perhaps only one small section was at, say, $\varepsilon = 2 \times 10^{-6} \text{ m}^2 \text{ s}^{-3}$ and the rest of the water column was of the order of $\varepsilon = 10^{-8} \text{ m}^2 \text{ s}^{-3}$.

Energy dissipation—If the observed layers of mixing fluid extend across the entire lake, then taking a dissipation rate within a layer to be $\varepsilon = 10^{-7} \text{ m}^2 \text{ s}^{-3}$, the total rate of energy dissipation to heat E' (Watts) is $\rho V \varepsilon$, where ρ is density and V is volume of the layer. If we assume a lake with an equivalent circular diameter d (at the depth of the pycnocline) of 1,500 m sustains a 0.25-m-thick turbulent layer covering say 1/10 of this area, the layer should dissipate around 4 W. We now seek sources for this energy.

A number of mechanisms might have generated the turbulent layers, including double diffusion and groundwater buoyancy inflow effects, direct wind mixing, direct sidewall

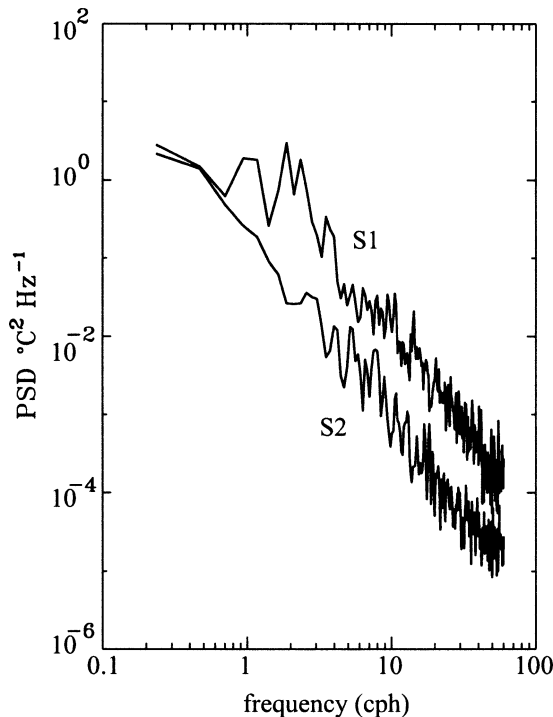


Fig. 8. Spectra derived from temperature timeseries from S1 (7.55 m depth) and S2 (6.5 m depth).

mixing, and internal wave-driven shear instability. While double diffusion can generate convectively-driven layering (e.g., Ruddick 1983), favorable conditions were found only on the top side of the pycnocline. Groundwater inflows of seawater would have generated a clear temperature–salinity signature. All remaining potential layer-forming mechanisms have some link to internal wave processes, so it is useful to consider the internal wave climate in the pit lake.

The pit lake sustains a continuous spectrum of internal waves (Fig. 8). The periods of the dominant temperature fluctuations were 60 and 30 min. These waves are a basin-scale baroclinic response to wind events and persist for many days (Fisher 2002). There is clearly a continuous tail representing a spectrum of smaller amplitude waves at increasingly higher frequencies. The upper limit, set by the buoyancy frequency, is quite high due to the strength of the stratification and will be around 20–50 cph in the region beneath the pycnocline. However, there is no clear cutoff in the spectral energy suggesting the presence of TKE. The implied pycnocline deflections of 0.1 m and a period of around 1 h (Fisher 2002) suggests very small vertical velocities, of the order of 10^{-4} m s^{-1} , generating shear of perhaps 10^{-3} s^{-1} .

Direct wind forcing—Direct wind mixing requires entrainment at the pycnocline due to either stirring or shear instability. A bulk Richardson number can be defined as $Ri_b = g' h_1 / (u^*)^2$, where $g' = (\Delta\rho/\rho)g$ and h_1 is the surface layer depth and u^* is a friction velocity in the water. This is the basis of one-dimensional entrainment models so that the stirring deepening of the pycnocline occurs at a normalized velocity $u_c/u^* \propto Ri^{-1}$ (Spigel and Imberger 1980). Here, we set

$h_1 = 8$ m, $g' = 0.14$ m s⁻², and $u^* = 0.01$ m s⁻¹ so that $Ri > 10,000$. Clearly, entrainment over the 3–5-m extent of the layered region would require weeks of constant wind. Similarly, it is possible to show that the interfacial shear at the pycnocline is unlikely to generate instability.

In addition to this scaling, the observations suggest any link between wind forcing and the turbulent layers is unlikely to be direct because of the intermediate quiescent layers. Furthermore, the dissipation rate was almost always weaker in the surface waters than beneath the pycnocline. The gradient Richardson number at the interface is very large due both to the strength of the stratification and the weak velocity shear (low wind and small interface deflections, e.g., Stevens and Lawrence 1997b).

Direct sidewall mixing—Sidewall turbulent boundary layers are of great significance when considering diffusion in larger basins (Taylor 1993; MacIntyre et al. 1999; Ledwell et al. 2000) and so are potentially of significance on the smaller scale considered here. The rate of working in the boundary layer can be estimated as $E' = \tau u A$, where the shear stress $\tau = 0.5\rho C_d u^2$ ($C_d \approx 10^{-3}$) and A is the area of the boundary layer. Assuming the boundary-layer feeding the turbulent layer is only as thick as the layer itself (d_1), a driving boundary layer speed derived from the rate of turbulent dissipation ε is $u = (\varepsilon d_1 / C_d)^{1/3}$, which yields around 0.05 m s⁻¹. Persistent circulatory velocities of this magnitude are unlikely, so ultimately, we must look to the internal wave climate.

The only way velocities of around 0.05 ms⁻¹ are likely to be generated in the present system is through interaction of a internal basin-scale seiche with the step structure. Fisher (2002) noted that “if the halocline coincided with a pit wall bench then much greater shoaling and energy dissipation would be expected.” If the interface, or the reasonably well-stratified fluid just beneath, is at the lip of the step, then the near-interface fluid will be constantly filling or draining across the bench top (Fig. 9). Thus, it is possible to generate enough TKE in the sidewall boundary layer; however, this energy has to propagate into the center of the pit lake unattenuated. Observations by Lemckert and Imberger (1995) of the decay of intrusions generated by a bubble plume suggest that this is not possible, so the turbulent layers in the center of the pit lake are not directly supplied by the turbulent fluid at the boundaries.

Basin-scale internal-wave instability—Shear instability driven by the large-amplitude basin-scale internal waves might potentially drive internal instability directly. It is possible that the observations are manifestations of the natural evolution of layering evolving as a consequence of basin-scale shear and stratification. Pelegrí and Sangrà (1998) consider diffusion of density and the formation of steps in the density structure. These are not seen here, although as the mixing is not produced everywhere, potentially the stratification adjusts sufficiently rapidly that these regions are only observed as the weak perturbations of Fig. 2.

At a fundamental level, there must be sufficient energy within the internal wave structure to drive the levels of mixing observed. The potential energy per unit width V in an

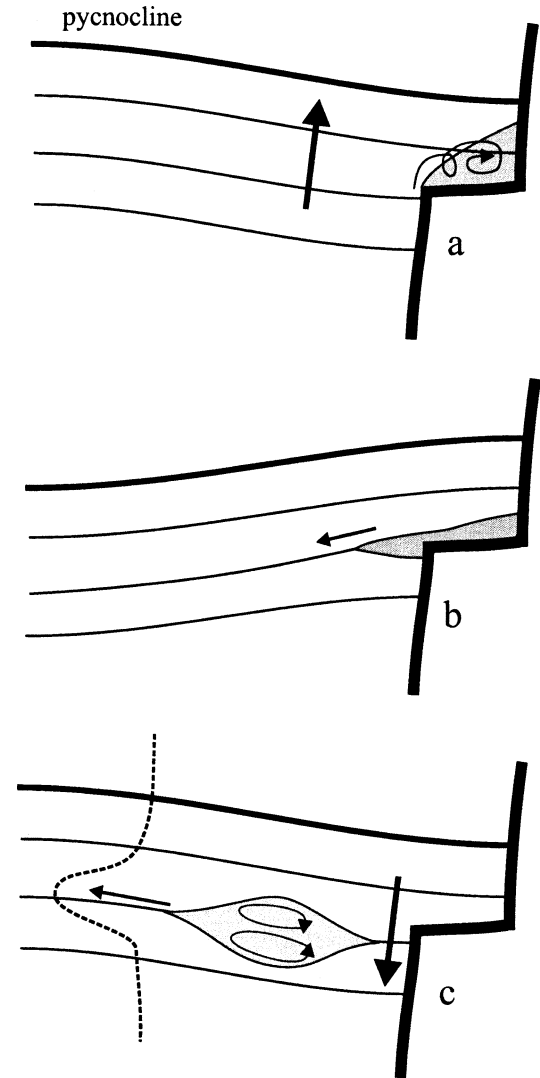


Fig. 9. Turbulence and internal wave generation at a sidewall step beneath the main pycnocline (bold, largely horizontal line). The panels show evolution in time, whereby, initially, in (a) the upward motion separates on the lip of the bench, creating a mixing region that then (b) consolidates and (c) flows out into the basin potentially in the form of a second-mode-like wave. The dashed line to the left in (c) is the likely horizontal velocity profile.

internal seiche setup can be estimated to be (Monismith 1985)

$$V = \frac{\Delta\rho g L^3 S^2}{24}$$

a function of the density difference $\Delta\rho$ (15 kg m⁻³), basin length L (~1,000 m), and interface slope S (0.1/1,000). If we assume a width of 1000 m and that the energy is lost in, say, 10 wave cycles (10 h; Fig. 8), this suggests a total energy loss rate of about 2 W, a comparable magnitude to that being dissipated here. However, the shear developed with such long wavelength waves is so small as to suggest instability unlikely. A more detailed consideration of the internal-wave dissipation over long timescales is developed by Fisher (2002).

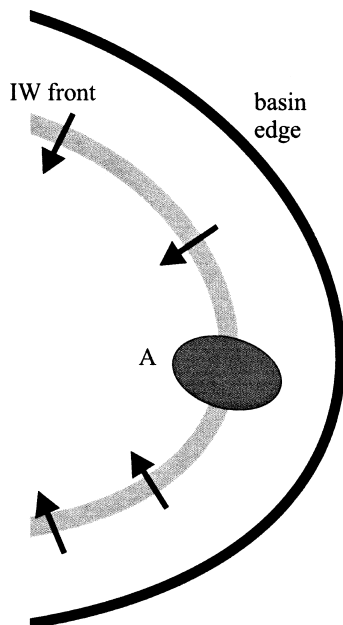


Fig. 10. Interpretive sketch showing internal wave (IW) front forced at the basin boundary and subsequently focused, creating regions of instability (A) at the locations of greatest curvature.

Further consideration of the persistence of the laminar layering (Fig. 3) shows that either the layers are destroyed and reformed rapidly or they have limited spatial extent. For example, in Fig. 4, by the time the initial wind event ceased (around decimal day 188.68) the relaminarization had already commenced. The laminar layer persisted for over an hour, during which time there were two velocity maxima in the hour-long internal wave that dominates the spectrum (Fisher and Lawrence in press). The return of the wind around 30 min later coincided with a weak return to a turbulent state until around an hour later (decimal day 188.73), but this was insufficient evidence to suggest a causal relationship.

Propagating internal wave-related shear—Shear is provided by short-wavelength internal waves that propagate away from the boundaries and potentially generate instability, as identified by Schmidt and Spiegel (2000) examining solitary waves formed by gravitational collapse of a packet of fluid. One of the unique characteristics of pit lakes is that, because of its regular and level bathymetric variations, a basin-scale internal wave will generate perturbations along the entire boundary at around the same time. Subsequently the energy is focused in both the vertical (through the stratification) and in the horizontal because the lake is roughly circular (Fig. 10). A simple appreciation of focusing is found by considering a wave front to be formed everywhere around the pit lake at once, akin to the reverse of a ripple-tank experiment. By the time the wave front is halfway to the center of the pit lake, this energy per unit length of wave front has doubled, so that at some point, conditions suitable for instability might be met.

By a process of reduction, it seems most likely that basin-scale internal waves generated, with the assistance of the

step structure, mixing directly at the sidewalls, but internal waves were required to propagate and interact to generate the interior mixing. More directed observation is required to confirm this, but it certainly illustrates the complex pathways for energy in limnetic systems.

Relevance to natural lakes—The spectrum of internal waves is not so different from a natural lake of this scale (e.g., Stevens 1999), although the strong stratification results in the waves being of relative high frequency. Mono Lake, although larger in area and shallower, has much in common with the Island Copper pit lake, as it too is strongly salt stratified and has been meromictic in the past (MacIntyre et al. 1999). This system also exhibits well-defined and rapid basin-scale internal-wave structure.

With regard to dissipation rates, it is apparent that the observed dissipation rate levels observed in the Island Copper energetic layers were relatively high compared with natural lakes (see Imberger and Ivey 1991; Wüest and Lorke 2003). The magnitude of ε observed here is more in tune with what one would expect in a lake surface layer, not beneath a very strong pycnocline that retards large-amplitude internal waves and vertical stirring. Certainly, other than right at the pycnocline and within the laminar regions separating the turbulent layers, the dissipation estimates indicated typical values of the buoyancy Reynolds number $\varepsilon/(\nu N^2) \sim 25$ ($\varepsilon = 10^{-7} \text{ m}^2 \text{ s}^{-3}$, $N^2 = 4 \times 10^{-3} \text{ rad}^2 \text{ s}^{-2}$), which just exceeds the critical value 20, defining active turbulence. Even taking into account the limited vertical extent of the profiles, this level of activity is very unusual for a lake (Saggio and Imberger 2001; Wüest and Lorke 2003). Although MacIntyre et al. (1999) found $\varepsilon > 10^{-7} \text{ m}^2 \text{ s}^{-3}$ at some times beneath the strong pycnocline in Mono Lake.

It seems unlikely that the behavior observed here would be clearly identified in a natural lake. First, the strong stratification and regular bathymetry (in both a horizontal and vertical extent) must play an important role in generation of the waves. If it did occur in a natural lake, it would likely be much more difficult to separate from other processes, as bathymetric variations are rarely so well defined as in the present situation (except perhaps small crater lakes, e.g., Chikita et al. 1993).

Despite the unlikelihood of the manifestation seen here appearing in a natural lake, it does allow us to speculate on the nature of sidewall versus internal-wave interaction (presumably shear)-driven turbulence. Time-averaged profiles of turbulence properties from S1 and S2 (Fig. 7) show a clear trend in the averaged data, whereby the sidewall data, for the same dissipation rate, exhibits a greater dissipation of thermal variance. The departure of the mean of Γ_d^0 from around 0.2 is presumably associated with the contribution to potential energy gain due to salinity. At each depth, assuming that the salinity profiles at S1 and S2 are comparable, the salinity contribution to potential energy gain should scale with the thermal contribution by the same amount. The present work suggests an inherent difference between friction-induced sidewall turbulence and the interior velocity shear-driven process. The lower χ_θ around the level of the sill at S1 relative to S2 for comparable levels of ε suggests a clear

difference in the dissipation ratio for wave-generated shear and direct boundary forcing of turbulence.

In summary, turbulence in this pit lake is unusual because these lakes often have relatively ordered bathymetry and are strongly stratified in both heat and salt. The observations show unexpectedly high turbulence beneath the pycnocline that was confined to thin layers around 0.25–0.5 m thick. While the highly turbulent layers appeared both near and far from sidewalls, the different dissipation ratios Γ_d^* suggest that there was some inherent difference in how the turbulence was manifest at the two locations. While the ultimate genesis of the layers lay in the basin-scale internal waves in conjunction with the sidewall step structure, the implication is that the different actual forcing process resulted in differences in the nature of the turbulence.

From the important perspective of quantifying turbulence and transport in pit lakes, it is clear that we have yet to fully appreciate the complexity and variety of behaviors brought on by these systems. While studies like MacIntyre et al. (1999) clearly identify the importance of boundary-layer processes, the present study indicates that the potential exists for such mechanisms to affect transport processes in the interior of the lake. Transport will always be limited by the slowest link. The very high-energy dissipation and concomitant diffusivity will enhance transport locally in the layers, but material will always come up against the near-molecular rates at the interface. Fickian diffusion across this interface involves both the diffusivity and the concentration gradient. So while enhanced transport deeper in the water column cannot influence the K_z right at the pycnocline, it can affect the supply and hence the local gradient of material concentration. More observational studies such as described here are required before we can build a reliable integrative picture sufficient to enable mass transport prediction over timescales of decades.

References

- BOEHRER, B., H. HEIDENREICH, M. SCHIMMELE, AND M. SCHULTZE. 1998. Numerical prognosis for salinity profiles of future lakes in the open cast mine Merseburg-Ost. *Int. J. Salt Lake Res.* **7**: 235–260.
- CHIKITA, K., Y. HOSOGAYA, AND S. NATSUME. 1993. The characteristics of internal waves in a caldera lake introduced from field measurements: Lake Kuttara, Hokkaido. *Jpn. J. Limnol.* **54**: 213–223.
- DILLON, T. M., AND D. R. CALDWELL. 1980. The Batchelor spectrum and dissipation in the upper ocean. *J. Geophys. Res.* **85**: 1910–1916.
- ETEMAD-SHAHIDI, A., AND J. IMBERGER. 2001. Anatomy of turbulence in thermally stratified lakes. *Limnol. Oceanogr.* **46**: 1158–1170.
- FISHER, T. S. R. 2002. Limnology of the meromictic Island Copper mine pit lake. Ph.D. thesis, Dept. Civil Engineering, Univ. of British Columbia.
- , AND G. A. LAWRENCE. In press. Development of the meromictic Island Copper mine pit lake for the treatment of acid rock drainage. *ASCE, J. Env. Eng.*
- GARGETT, A. E., AND J. N. MOUM. 1995. Mixing efficiencies in turbulent tidal fronts: Results from direct and indirect measurement of density flux. *J. Phys. Oceanogr.* **25**: 2583–2608.
- GRÄFE, H., B. BOEHRER, N. HOPPE, S. C. MÜLLER, AND P. HAUPTMANN. 2002. Ultrasonic in-situ measurements of density, adiabatic compressibility and stability frequency. *Limnol. Oceanogr.* **47**: 1255–1260.
- HAMBLIN, P. F., C. L. STEVENS, AND G. A. LAWRENCE. 1999. Simulation of vertical transport in a mining pit lake. *ASCE J. Hyd. Eng.* **125**: 1029–1038.
- IMBERGER, J., AND G. N. IVEY. 1991. On the nature of turbulence in a stratified fluid, part II: Application to lakes. *J. Phys. Oceanogr.* **21**: 659–680.
- IVEY, G. N., AND J. IMBERGER. 1991. The nature of turbulence in a stratified fluid, part I: The energetics of mixing. *J. Phys. Oceanogr.* **21**: 649–658.
- KARAKAS, G., I. BROOKLAND, AND B. BOEHRER. 2003. Physical characteristics of Acidic Mining Lake 111. *Aquatic Sci.* **65**: 297–307.
- KLAPPER, H., AND M. SCHULTZE. 1995. Geogenically acidified mining lakes—living conditions and possibilities for restoration. *Int. Revue ges. Hydrobiol.* **80**: 639–653.
- KOCIS, O., H. PRANDKE, A. STIPS, A. SIMON, AND A. WÜEST. 1999. Comparison of dissipation of turbulent kinetic energy determined from shear and temperature microstructure. *J. Mar. Syst.* **21**: 67–84.
- LEDWELL, J. R., E. T. MONTGOMERY, K. L. POLZIN, L. C. ST. LAURENT, R. W. SCHMITT, AND J. M. TOOLE. 2000. Evidence for enhanced mixing over rough topography in the abyssal ocean. *Nature* **403**: 179–182.
- LEMCKERT, C., AND J. IMBERGER. 1995. Turbulence within inertia-buoyancy balanced axisymmetric intrusions. *J. Geophys. Res.* **100**: 22649–22666.
- MACINTYRE, S., K. M. FLYNN, R. JELLISON, AND J. R. ROMERO. 1999. Boundary mixing and nutrient fluxes in Mono Lake, California. *Limnol. Oceanogr.* **44**: 512–529.
- MONISMITH, S. G. 1985. Wind-forced motions in stratified lakes and their effect on mixed layer shear. *Limnol. Oceanogr.* **30**: 771–783.
- MOUM, J. N. 1996. Efficiency of mixing in the main thermocline. *J. Geophys. Res.* **101**: 12057–12069.
- NASH, J. D., AND J. N. MOUM. 2002. Microstructure estimates of turbulent salinity flux and the dissipation spectrum of salinity. *J. Phys. Oceanogr.* **32**: 2113–2130.
- OAKEY, N. S. 1982. Determination of the rate of dissipation of turbulent energy from simultaneous temperature and velocity shear microstructure measurements. *J. Phys. Oceanogr.* **12**: 256–271.
- OSBORN, T. R. 1980. Estimates of the local rate of turbulent diffusion from dissipation measurements. *J. Phys. Oceanogr.* **10**: 83–89.
- PELEGRÍ, J. L., AND P. SANGRÀ. 1998. A mechanism for layer formation in stratified geophysical flows. *J. Geophysical Res.* **103**: 30679–30693.
- RUDDICK, B. 1983. A practical indicator of the stability of the water column to double-diffusive activity. *Deep-Sea Research* **30**: 1105–1107.
- , A. ANIS, AND K. THOMPSON. 2000. Maximum likelihood spectral fitting: The Batchelor spectrum. *J. Atmos. Oceanic Tech.* **17**: 1541–1555.
- , D. WALSH, AND N. OAKEY. 1997. Variations in the apparent mixing efficiency in the North Atlantic central water. *J. Phys. Oceanogr.* **27**: 2589–2662.
- SAGGIO, A., AND J. IMBERGER. 2001. Mixing and turbulent fluxes in the metalimnion of a stratified lake. *Limnol. Oceanogr.* **46**: 392–409.
- SANDERSON, B., K. PERRY, AND T. PEDERSON. 1986. Vertical diffusion in meromictic Powell Lake, British Columbia. *J. Geophys. Res.* **91**: 7647–7655.
- SCHMIDT, N. P., AND R. H. SPIGEL. 2000. Second mode internal

- solitary waves I—integral properties, p. 809–814. *In* Proceedings 5th International Stratified Flows Symposium, Vancouver, Canada, July 2000, Vol II.
- SHARPLES, J., M. J. COATES, AND J. E. SHERWOOD. 2003. Quantifying turbulent mixing and oxygen fluxes in a Mediterranean-type, microtidal estuary. *Ocean Dynamics* **53**: 126–136, DOI: 10.1007/s10236-003-0037-8.
- SHERMAN, J., AND R. E. DAVIS. 1995. Observations of temperature microstructure in NATRE. *J. Phys. Oceanogr.* **25**: 1913–1929.
- SPIGEL, R. H., AND J. IMBERGER. 1980. The classification of mixed-layer dynamics in lakes of small to medium size. *J. Phys. Oceanogr.* **10**: 1104–1121.
- SRDIC-MITROVIC, A. N., N. A. MOHAMED, AND H. J. S. FERNANDO. 1999. Gravitational settling of particles through density interfaces. *J. Fluid Mech.* **381**: 175–198.
- ST. LAURENT, L., AND R. W. SCHMITT. 1999. The contribution of salt fingers to vertical mixing in the North Atlantic Tracer Release Experiment. *J. Phys. Oceanogr.* **29**: 1404–1424.
- STEVENS, C. L. 1999. Internal waves in a small reservoir. *J. Geophysical Res.* **104**: 15777–15788.
- . 2003. Turbulence in an estuarine embayment: Observations from Beatrix Bay, New Zealand. *J. Geophys. Res.* **108**, DOI: 10.1029/2001JC001221.
- , AND G. A. LAWRENCE. 1998. Stability and meromixis in a water-filled mine pit. *Limnol. Oceanogr.* **43**: 946–954.
- , AND ———. 1997a. The effect of sub-aqueous disposal of mine tailings in standing waters. *IAHR J. Hydraul. Res.* **32**: 1–13.
- , AND ———. 1997b. Estimation of wind-forced internal seiche amplitudes in lakes and reservoirs, with data from British Columbia, Canada. *Aquatic Sci.* **59**: 115–134.
- TAYLOR, J. R. 1993. Turbulence and mixing in the boundary layer generated by shoaling internal waves. *Dyn. Atmos. Oceans* **19**: 233–258.
- WÜEST, A., AND A. LORKE. 2003. Small-scale hydrodynamics in lakes. *Annu. Rev. Fluid Mech.* **35**: 373–412, DOI: 10.1146/annurev.fluid.35.101101.161220.

Received: 27 January 2004

Accepted: 16 July 2004

Amended: 13 August 2004